Shahrood University of Technology
Iranian Society of Mining Engineering (IRSME)
Journal of Mining and Environment (JME)
journal homepage: www.jme.shahroodut.ac.ir
THOMSON REUTERS
Vol. 10, No. 3, 2019, 679-694.
DOI: 10.22044/jme.2019.7941.1661

Geostatistical estimation to delineate oxide and sulfide zones using geophysical data; a case study of Chahar Bakhshi vein-type gold deposit, NE Iran

H. Azmi*, P. Moarefvand and A. Maghsoudi

Department of Mining and Metallurgy Engineering, Amirkabir University of technology (Tehran Polytechnic), Tehran, Iran

Received 2 January 2019; received in revised form 25 February 2019; accepted 13 March 2019

Keywords

Oxide and Sulfide Zones

Geophysical Model

Vein-Type Gold Deposit

Ordinary Kriging

Abstract

Delineation of oxide and sulfide zones in mineral deposits, especially in gold deposits, is one of the most essential steps in an exploration project that has been traditionally carried out using the drilling results. Since in most mineral exploration projects there is a limited drilling dataset, application of geophysical data can reduce the error in delineation of the sulfide and oxide zones. For this purpose, we produced a 3D model of Induced Polarization (IP) data using the ordinary kriging technique. Then the modelling results were compared with the drilling data. The results obtained showed that the 3D geophysical models would properly delineate the sulfide and oxides zones. This work presents a new application of the IP results for separation of these zones. In addition, the conducted variography in this work suggests reducing the profile spacing of dipole-dipole IP arrays down to 25 m. This would properly enrich the integration of geophysical and geological results in the modelling of gold deposits.

1. Introduction

The delineation of sulfide and oxide zones during a reserve estimation is an essential problem for designing a mineral processing plant. The geological datasets used for zone delineation in mineral deposits are usually based on mineralogy, petrography, and the study of grades and alteration mineral assemblages [1-5]. In addition, fluid inclusion studies. (e.g. [6-9]) and ^{34}S isotope investigations (e.g. [10]) are other methods that have been used for separation of different zones in mineral deposits. Gold deposits are highly variable in form, ranging from thin quartz veins to large disseminated deposits, and are located in a variety of geological environments. Consequently, they exhibit a wide range of geophysical signatures. Geophysical methods and tools including different techniques such as magnetic, self-potential, induced polarization (IP), and resistivity are important techniques in mineral exploration [11-18]. It is almost impossible to get a direct geophysical response from gold because of the low grades in deposits, except when electromagnetic detectors are used for individual shallow nuggets. However, indirect geophysical indications may occur through association of gold with particular host rocks, marker beds or structures that are, for example, of unusual magnetization, density, electric polarization or conductivity–resistivity [19-20] Resistive gold-bearing silicified zones and shallow quartz vein systems are commonly detectable by conventional galvanic or inductive resistivity techniques [21].

There are many techniques that estimate or simulate the geosciences datasets. For instance, geostatistical techniques are widely used in geophysical mineral explorations [22-28].

Delineation of oxide and sulfide zones has been traditionally carried out using the drilling results. The present work focused on using geological, dipole–dipole IP data through geostatistical processing to separate sulfide and oxide zones at

* Corresponding author: azmi@aut.ac.ir (H. Azmi).

the Charbakhshi gold deposit in NE Iran. To the best of our knowledge, so far, no specific research work has been carried out to use the IP data in the separation of sulfide-oxide zones in gold deposits. The integration geophysical data with the existing drilling data can help engineers separate the sulfide and oxide zones more precisely. Therefore, in this work, we tried to present a new application of IP results for separation of these zones.

2. Case study and geological setting

The Chahar Bakhshi area is located in the north of the Kaboodan Village, 14 km north of the Bardaskan City, in Khorasan-e-Razavi Province (Figure 1). From the geological viewpoint, the Precambrian Taknar Formation is the most dominant outcropped unit in the studied area. It consists of green schist associated with meta-rhyodacite and meta-rhyolite layers, and submarine acidic tuffs. The Taknar Formation in this area is more than 2000 m thick, and it has experienced a weak metamorphism. In the west of the area of interest, the relatively large outcrops of granitic (Precambrian) and gabbro-dioritic (Tertiary) rocks have intruded the Taknar Formation. In addition, thick limestone units (Cretaceous) and the Kerman conglomerate (Paleocene) outcropped in the north of the studied area. Smaller parts of the Soltanieh dolomitic formation (Cambrian) outcrop in SE and NW of the area as well. Copper oxide and sulfide mineralization occur in chloritic, sericitic, and kaolinitic zones. Moreover, the silicification and kaolinitization as well as iron oxides occur in other parts, and the iron caps form on sericitic zones [29, 30]. Figure 2 shows the details of geological units. The location of the conducted dipole-dipole arrays and the outcropped mineralization are illustrated in this figure as well.

3. Methods

The methods used in this work include two parts. The main part involves the geostatistical processing on geophysical data including data checking and data selection, preparing a block model, variography, and estimation. The 3D geophysical model is the result of this part. The second part uses the borehole geological logs to validate the model. Figure 3 illustrates the workflow (methods and stages) chart of the current work. After the data selection step, a data variography was carried out. Afterwards, a block model of an estimation space was created as the basis of kriging estimations. Next the ordinary kriging (OK) technique was applied on the data over the estimation space to create a 3D model of the IP values. OK operates under simple assumptions of stationary, and requires no knowledge of the average. Assuming that the region is a second-order stationary space, the OK method implicitly evaluates the mean in a moving neighborhood, and thus minimizing the estimation variance [33]. The estimation results were later validated and then used in the preparation of 3D geophysical models. The model was integrated with borehole geological logs to delineate the sulfide and oxide zones.

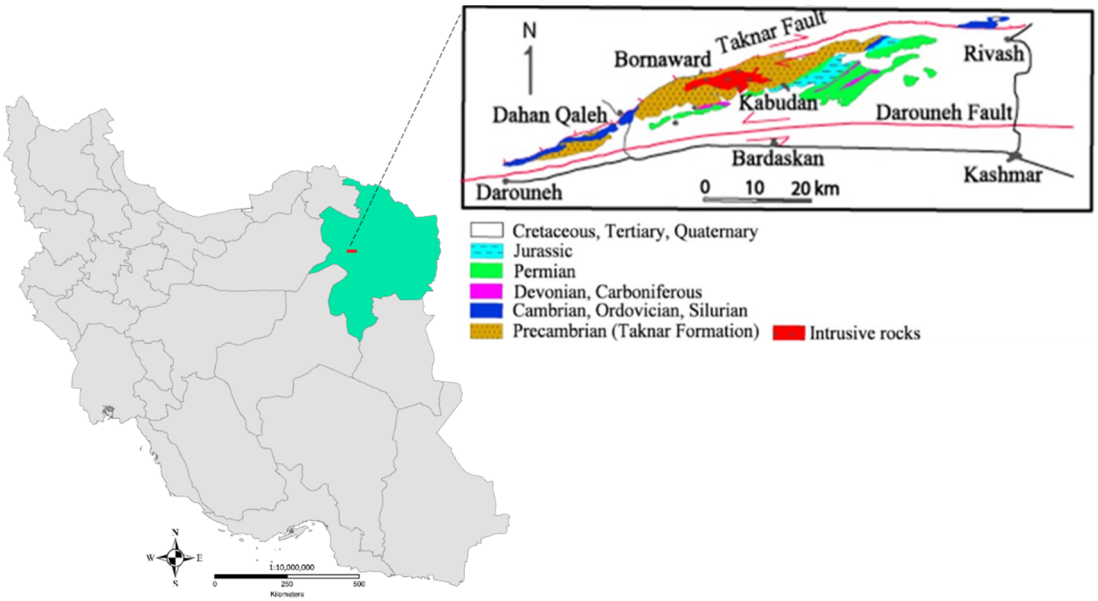

Figure 1. Geographical location of the studied area (modified from [31]).

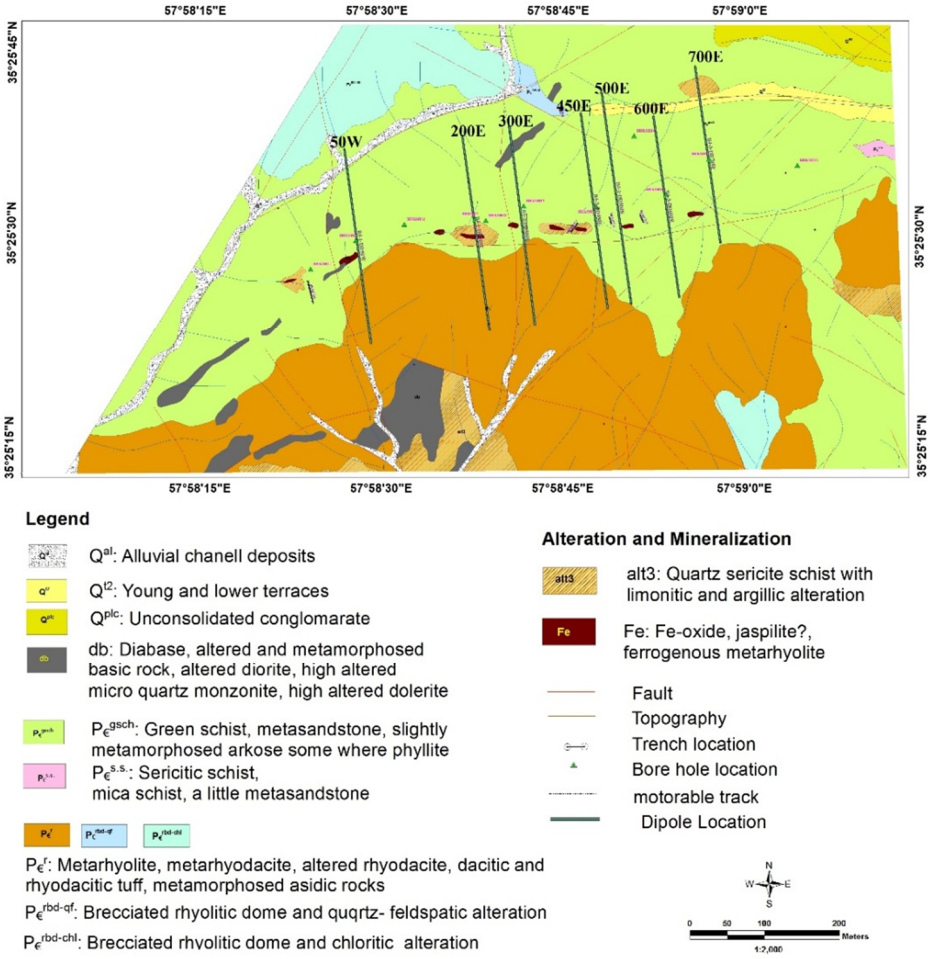

Figure 2. Geological map of the studied area and dipole-dipole location [32].

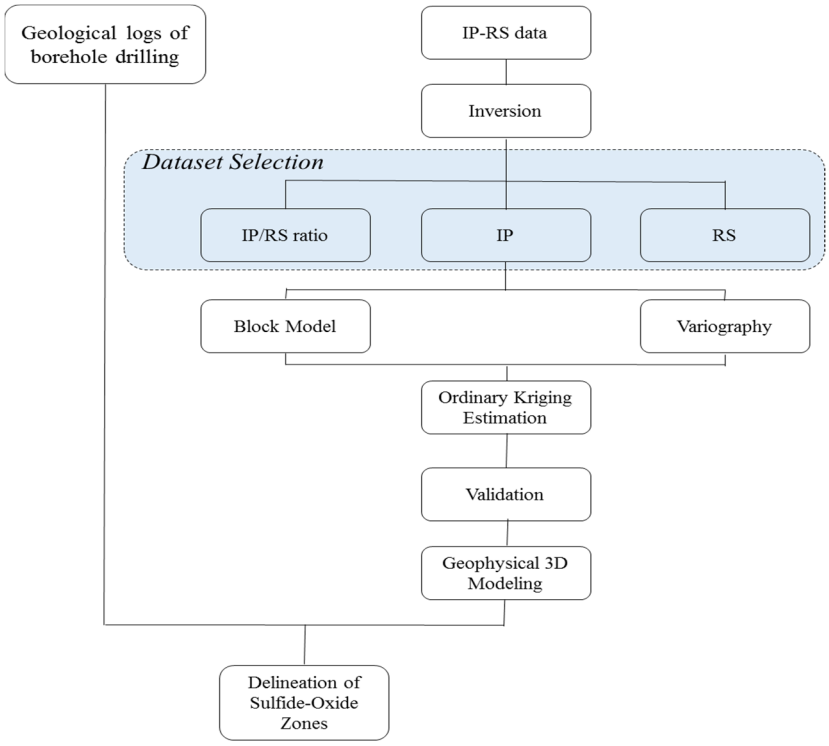

Figure 3. Workflow chart of the current study.

4. Results and discussion

4.1. Data selection

In this work, the geophysical dataset includes the IP and resistivity imaging data obtained from seven profiles of dipole-dipole array reported by [34]. In this array, the electrode spacing value was 20-40 m, and the profile spacing varied between 50 and 250 m (Table 1). The location of arrays is shown on the geological map of the area in Figure 2. The geophysical data consists of 3270 points generated by dipole-dipole chargeability and resistivity techniques. The 2D chargeability model of field surveys was obtained through the inversion functions.

In order to select the most appropriate data for later analyses, the resistivity, chargeability, and the chargeability to resistivity ratio sections were drawn. The results, in conjunction with field investigations, show that the IP data best separates the sulfide anomalies. Therefore, in this work, the chargeability data was selected for further processes. For instance, Figure 4 shows the prepared sections for Profile DD 450E. In addition, Figure 5 presents the histogram of IP imaging data. The important statistical characteristic of this histogram includes the number of data, mean, standard deviation, skewness, kurtosis, minimum, and maximum, which are equal to 3270, 6.1, 4.9, 1.7, 3.4, 0.19, and 33.7, respectively.

Table 1. Array configuration.

No	Profile name	Survey area		Electrode spacing	Dipole lag
1	DD50W	420N	60N	20-40 M	20 M
2	DD200E	480N	40N	20-40 M	20 M
3	DD300E	500N	140N	40 M	20 M
4	DD450E	500N	60N	20-40 M	20 M
5	DD500E	540N	80N	40 M	20 M
6	DD600E	520N	100N	40 M	20 M
7	DD700E	540N	80N	40 M	20 M

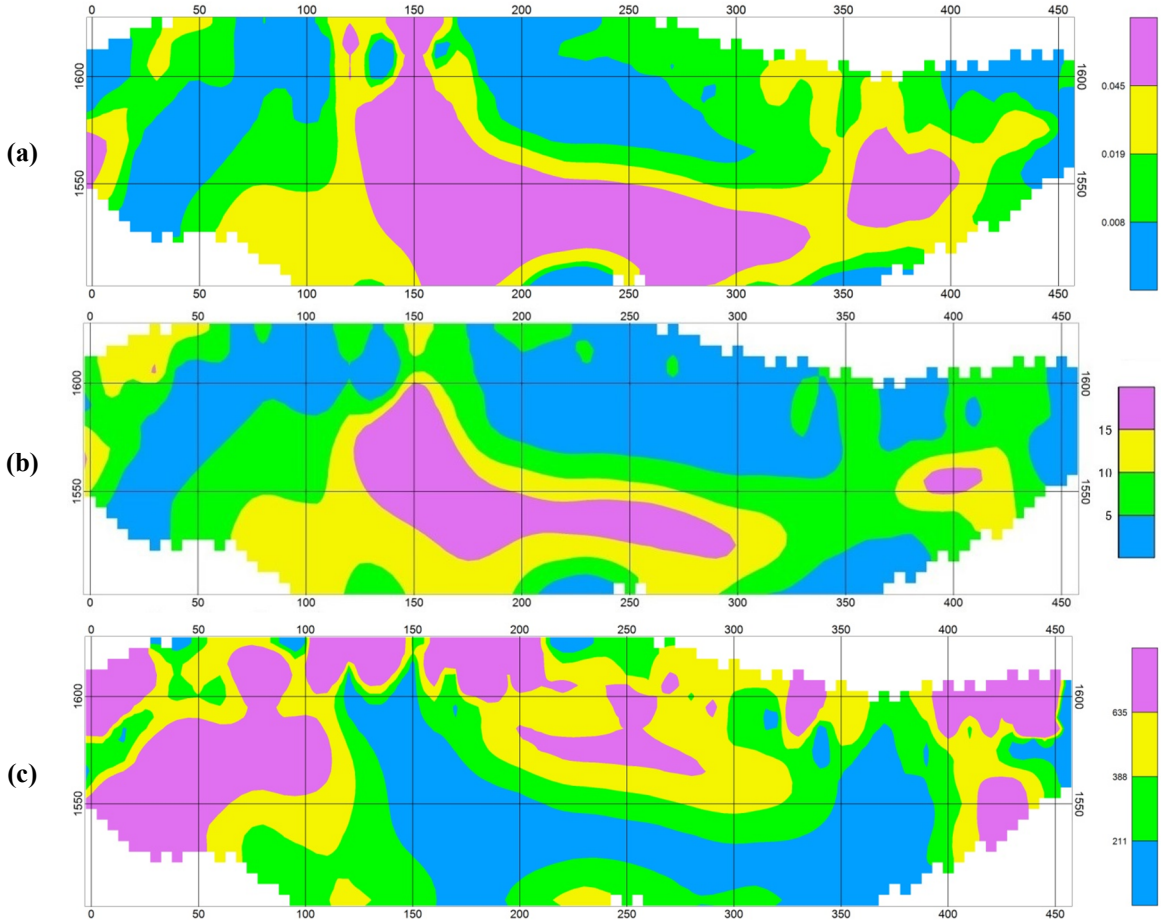

Figure 4. Profile DD-450E. (a) IP to resistivity ratio section; (b) IP section; and (c) resistivity section.

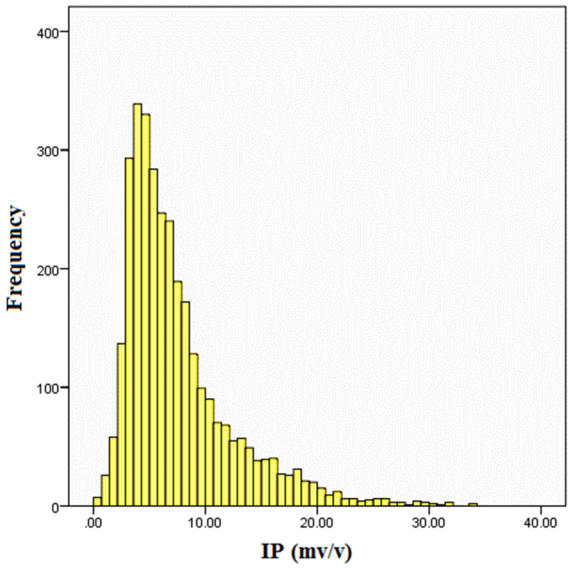

Figure 5. Frequency histogram of IP data.

4.2. Variography

A variogram is a structural analysis tool, and it is the first step in a geostatistical process through using regional variables [35]. In geostatistics, the location of points relative to each other is very important. The variogram is plotted based on sample locations and the differences between the values [36-38]. In this work, the variography process was conducted on the IP data in different directions. The results of the main directions are illustrated in Figure 6. As shown in this figure, the red-colored variogram was drawn along the profiles and perpendicular to the mineralization. The gray variogram is an omni-directional, and the green one is along the mineralization.

The variogram parallel to the profiles matches the omni-directional one but it does not show a hole-effect. Based on the dataset jumps from one profile to another, the omni-directional variogram shows a hole-effect. The variogram along the mineralization, however, is 100% stochastic (pure nugget). Since the dipole-dipole arrays were implemented on the same direction and perpendicular to the mineralization, the acquired data was already directional. The data along the mineralized zones had a larger distance. If the profile spacing was smaller, considering the geological nature of the mineralization, the variogram would be anisotropic.

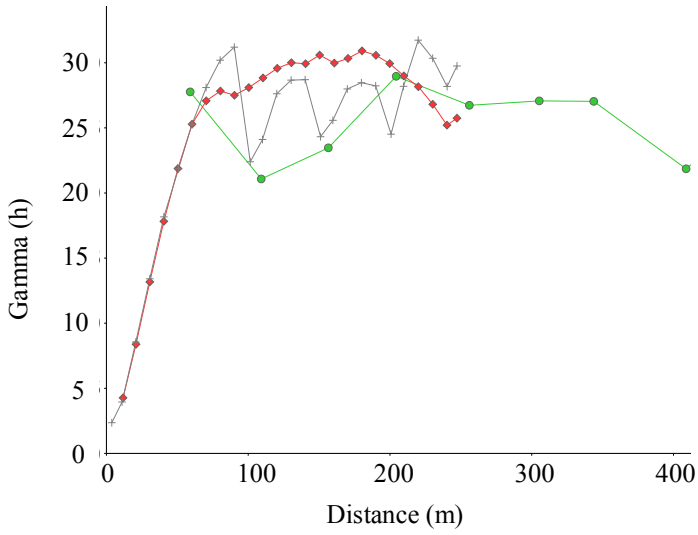

Figure 6. Various variograms of IP data.

It should be noted that the data of each single profile was recorded on the same direction with a profile spacing of 50–250 m, which is considered a large spacing in respect with the mineralization type (Table 1). Therefore, we used the omni-directional variogram to estimate the IP data. Figure 7 illustrates the variogram of the whole IP dataset. As shown, the variogram curve for the first 100 m represents a single structure. As the variography window moves toward farther profiles, the data of those profiles affect the variogram, which is depicted as if there is another structure. In fact, such identical fluctuations in a variogram curve is caused by the repetition of the same structure, and is called hole-effect [39].

Finally, an experimental spherical model was fitted on this variogram. This model shows a nugget effect of 2.3, a sill of 27, and a range of 100 m.

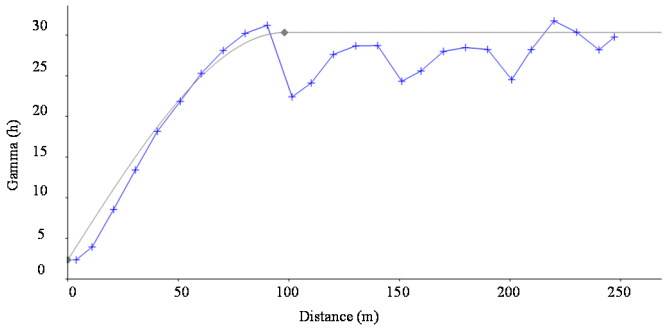

Figure 7. Variogram model of IP data.

4.3. 3D Modeling using OK

The estimation phase consists of four basic steps: theoretical geostatistics, data processing, kriging, and estimation [40]. Kriging requires an estimation space, which is determined using block models. These models are the basis of data analysis. In this work, the block model was produced using the geophysical data, topography of the area of interest using the cell size selection approach. According to the data spacing and the thickness of the mineralization, a cell size of 5 × 5 × 5 m was chosen for the modelling blocks.

The estimation process is conducted after preparing the estimation space (block model). In this work, considering the fact that the mean value was unknown, the ordinary kriging (OK) method was used to transform the 2D data into a 3D space, assuming a normal distribution for the IP data (see Figure 5). Having conducted the estimation process, a total of 65535 data cells were estimated. The histogram of the estimation results is shown in Figure 8. Important statistical properties of the estimated IP data include the number of data, mean, standard deviation, skewness, kurtosis, minimum, and maximum, which are equal to 65535 (number of block), 7.5, 3.79, 1, 1, –1, and 32, respectively.

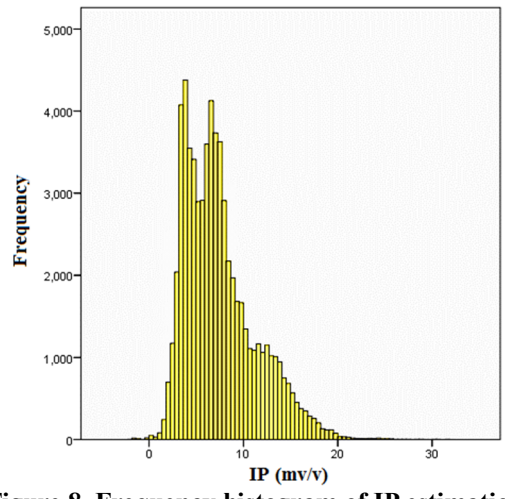

Figure 8. Frequency histogram of IP estimation data.

4.4. Cross-validation

The cross-validation is a tool to verify the accuracy of estimation conditions based on the estimations made at the given points. Variogram is the only tool available to represent the type of spatial change of selected samples from a population [39]. Sometimes the samples do not represent the actual conditions of spatial variables, and only the other samples of the population can satisfy the conditions. To understand how good an estimation method can express the spatial changes of a variable, one has to evaluate the validity of the estimation method used. In the validation process, the value of a sample is eliminated and then the value of that sample is estimated using the surrounding samples through the estimation method. Based on the results, the uncertainty (error value) is determined for that sample. Figure 9 shows the cross-validation of the IP data, in which the estimated value is close to the real data. This means that the estimation has been conducted properly.

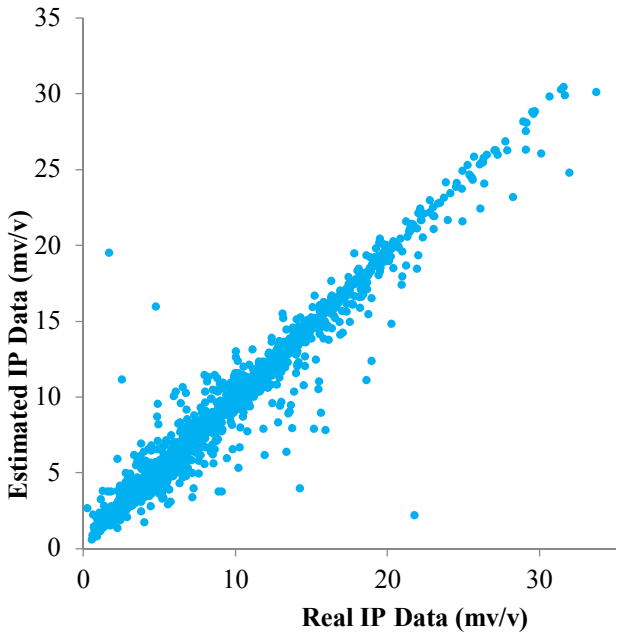

Figure 9. Cross-validation diagram of the IP data.

4.5. Delineation of sulfide and oxide zones and comparison with borehole loggings

Usually the boundary between the oxide and sulfide zones is determined based on the existing boreholes and their logging data. The drilling data shows the information related to the drilling station. If a sulfide zone is observed in a specific depth of a borehole, the zone would exist in the upper levels as well. Suppose that the drilling is being carried out on two topographical levels. If a borehole drilled in a higher altitude cuts an oxide zone at a depth of 30 m, for example, and a borehole drilled in a lower altitudes cuts a sulfide zone at 60 m, one can expect to find the oxide-sulfide boundary at a depth between 30 m and 60 m. However, it should be noted that in most of the deposits, due to financial considerations, the drilling is carried out only on one topographical level. Since geophysical data is affordable and continuous, it can facilitate this challenge. The comparison of this data with the drilling logs can suggest a given value to the delineation of sulfide and oxide zones. Obviously, this value is not certain and can change depending on the geophysical instruments and the geological nature of deposits.

In this work, the 3D geophysical model of the data was prepared using the geostatistical processes (Figure 10). According to the experimental and drilling data, a value of 12 mV/V was selected for the chargeability variable, based on which the sulfide and oxide zones were discriminated.

In order to provide a detailed perspective of the model, multiple sections along and perpendicular to the mineralization were drawn. Figure 11 depicts the location of the drawn sections.

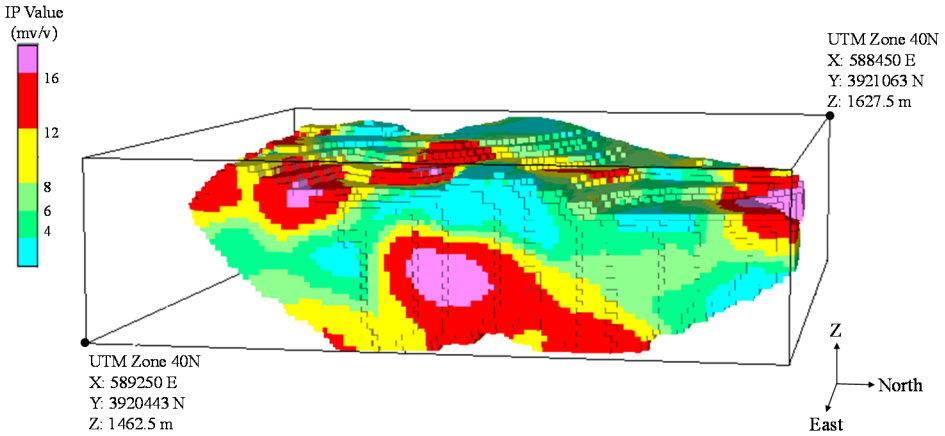

Figure 10. Block model of the deposit. The red and purple colors show the sulfide zone.

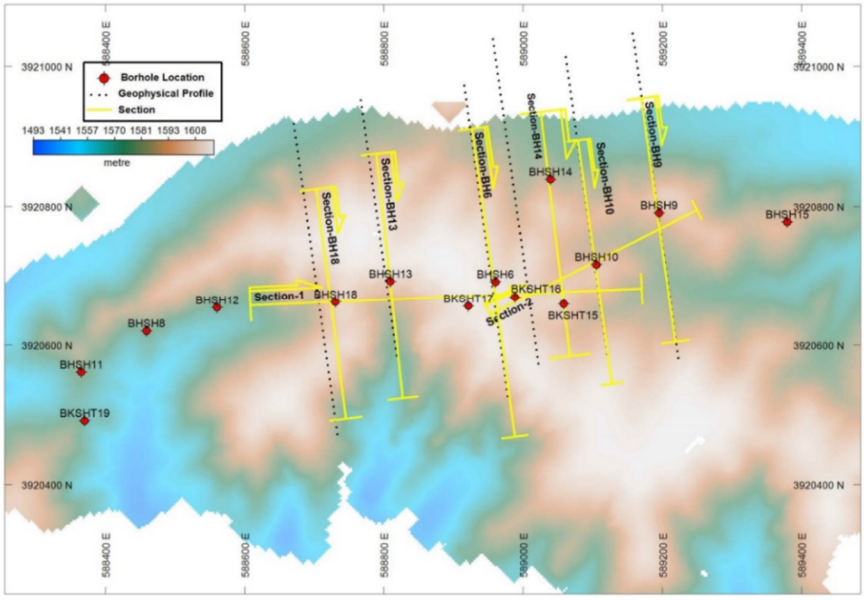

Figure 11. The location of six sections perpendicular to, and two sections along, the mineralization on the topographic map. The red points show the location of drilled boreholes and excavated trenches.

Figures 12-17 show the results of model validation using the boreholes. In all these figures, the dark black line on the geological log represents the mineralized zone. The red-colored box on the logs shows the sulfide zone. These zones contain mainly pyrite and rarely chalcopyrite.

In this work, the drilling log data was used to determine the proper value for delineation of the sulfide and oxide zones. Sections 1 and 2 (Figure18) were drawn along the mineralized zone. The red and purple colors represent the sulfide zones.

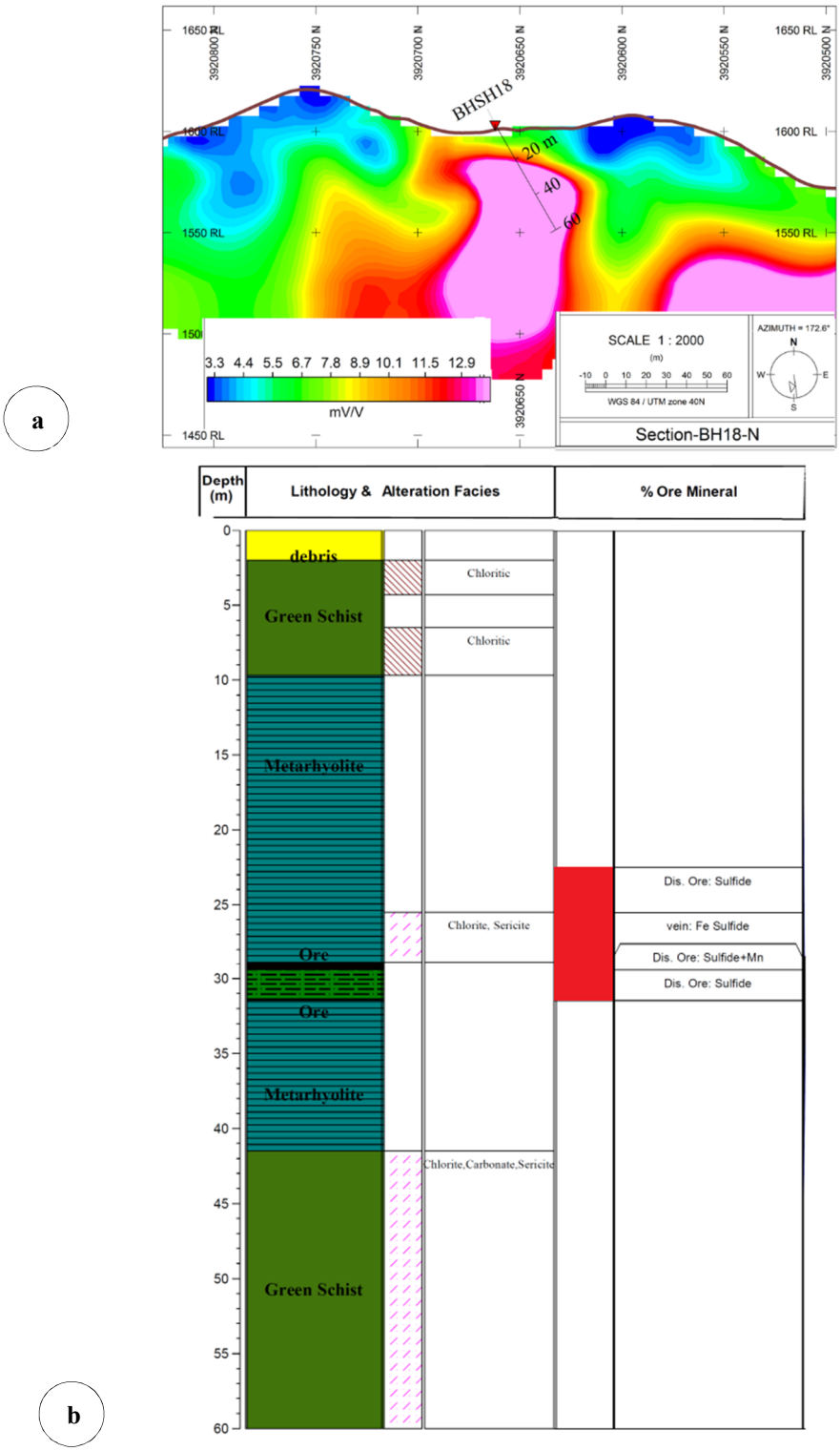

Figure 12. (a) 2D model of IP values and (b) geological log of borehole No. 18 and its corresponding mineralized zones (modified from [32]). As it is shown, the sulfide and mineralized zones lie at the depths of 22 until 32 m and 29 until 31 m, respectively. This means that the geological log confirms the model in the IP section. *Dis:* disseminated sulfide.

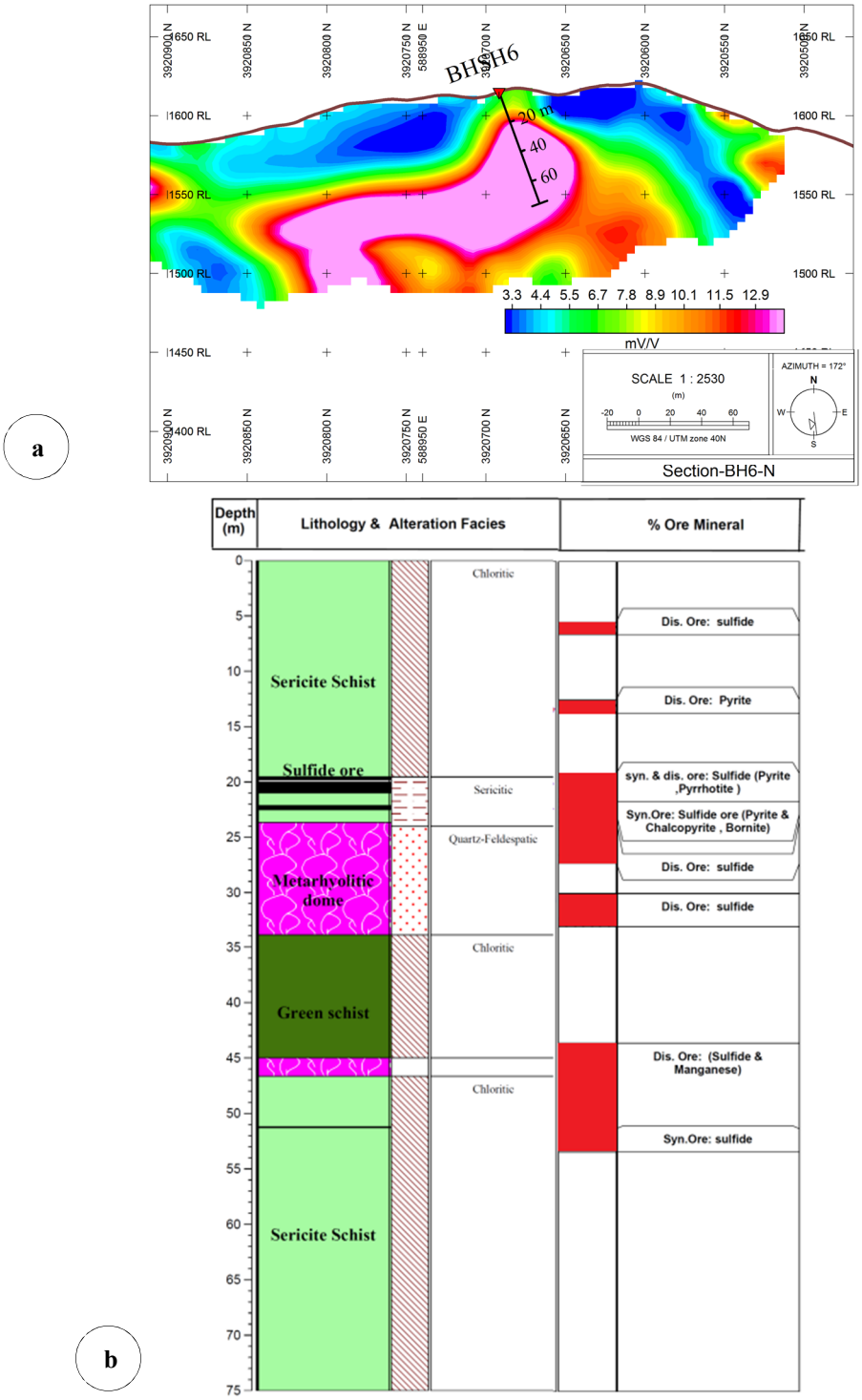

Figure 13. (a) 2D model of IP values and (b) geological log of borehole No. 6 and its corresponding mineralized zones (modified from [32]). As seen, the red-colored box on the logs shows the sulfide zone. The mineralized zones lie at the depths of 19 until 23 m. Therefore, the geological log confirms the presence of an ore zone in a depth of about 20 m that is shown in the IP section. *Dis:* disseminated sulfide; *Syn*: Syngenetic.

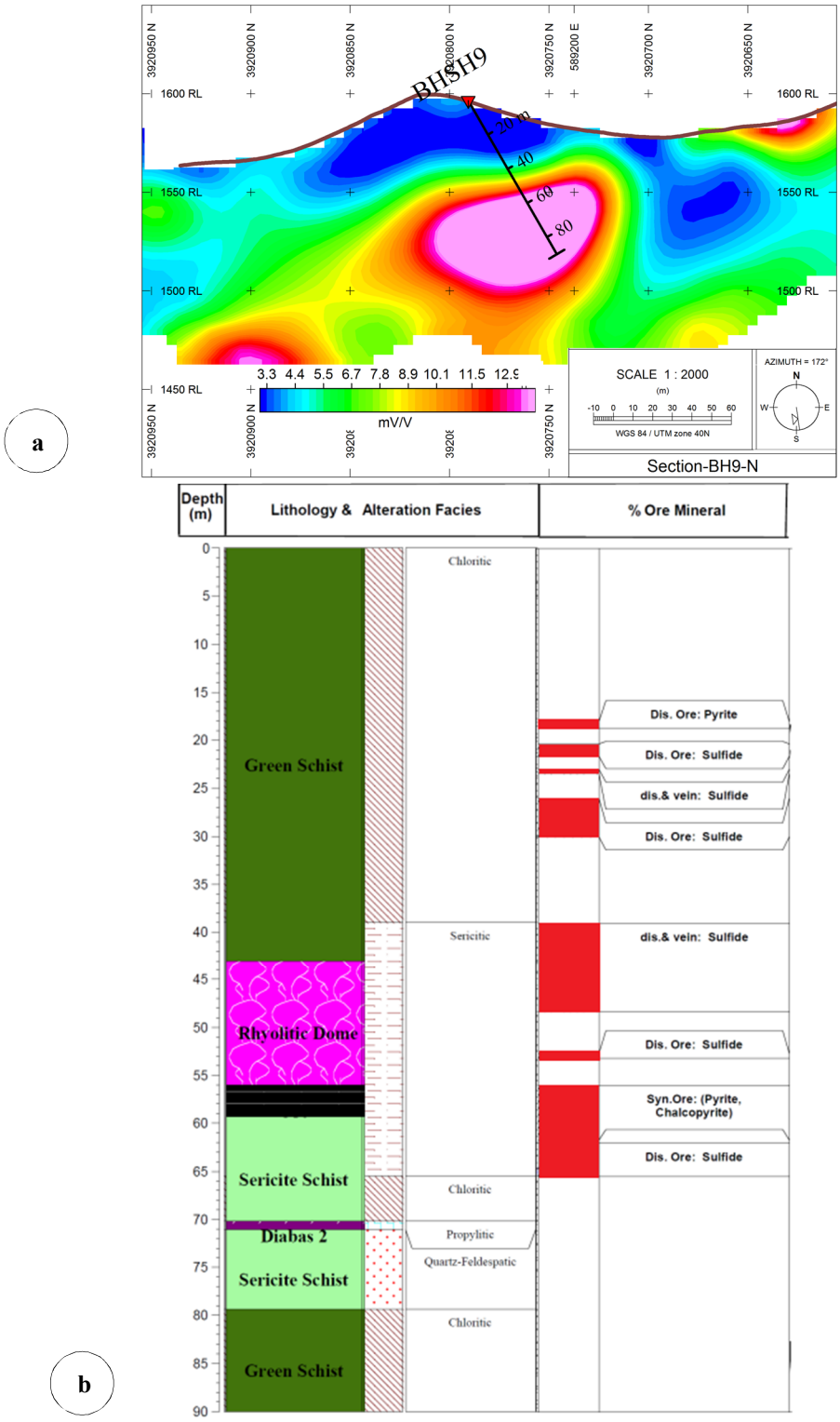

Figure 14. (a) 2D model of IP values and (b) geological log of borehole No. 9 and its corresponding mineralized zones (modified from [32]). As shown, the red-colored box on the logs shows the sulfide zone. The geological log confirms the presence of an ore zone in a depth of about 56 until 59 m that is shown in the IP section. *Dis:* disseminated sulfide; *Syn*: Syngenetic.

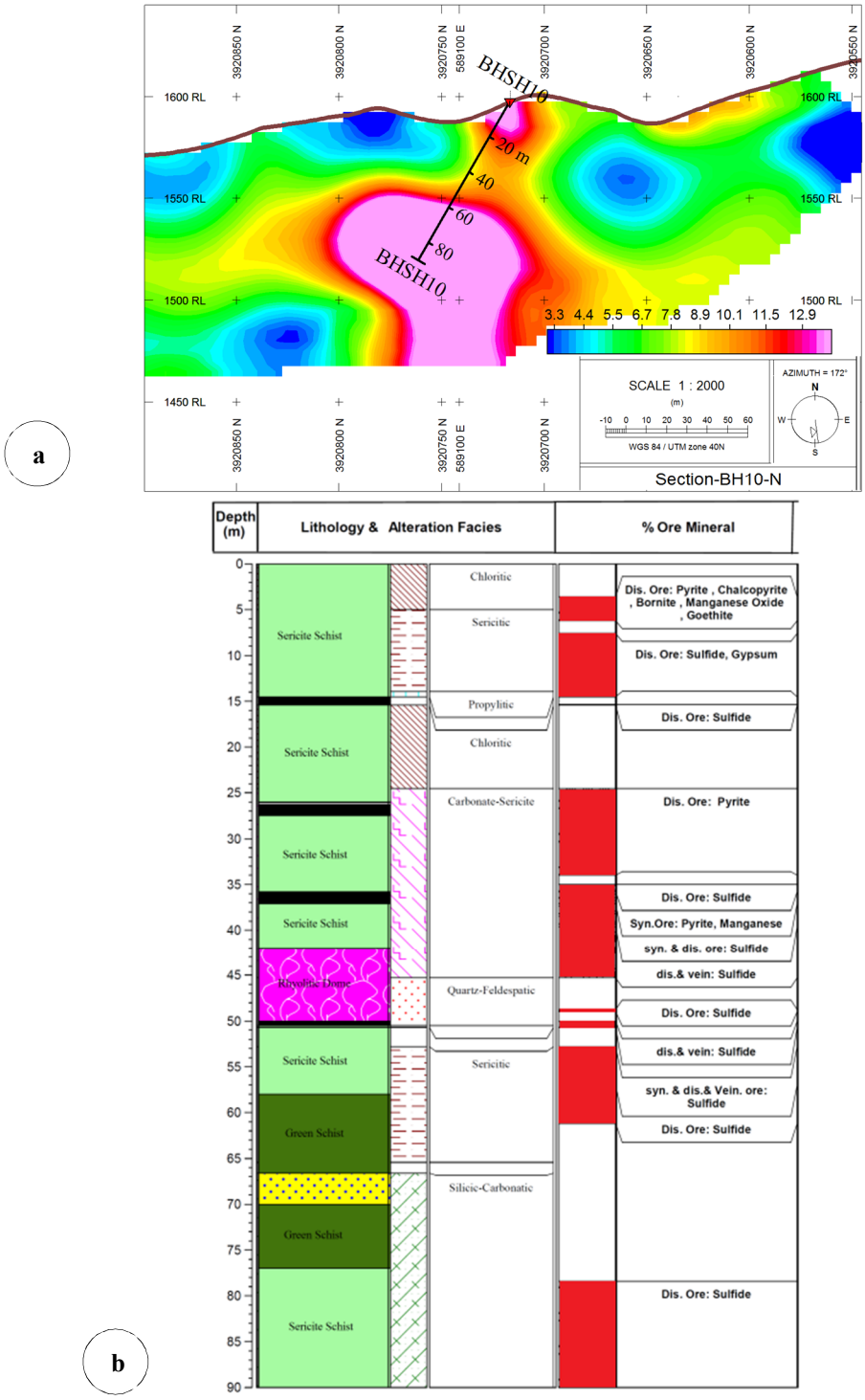

Figure 15. (a) 2D model of IP values and (b) geological log of borehole No. 10 and its corresponding mineralized zones (modified from [32]). As seen, the red-colored box on the logs shows the sulfide zone. The mineralized zones lie at the depths of 15,26,36,51 m. Therefore, the geological log confirms the presence of ore sulfide zone starting from the surface down to 90 m, which is also shown in the IP section. *Dis:* disseminated sulfide; *Syn*: Syngenetic.

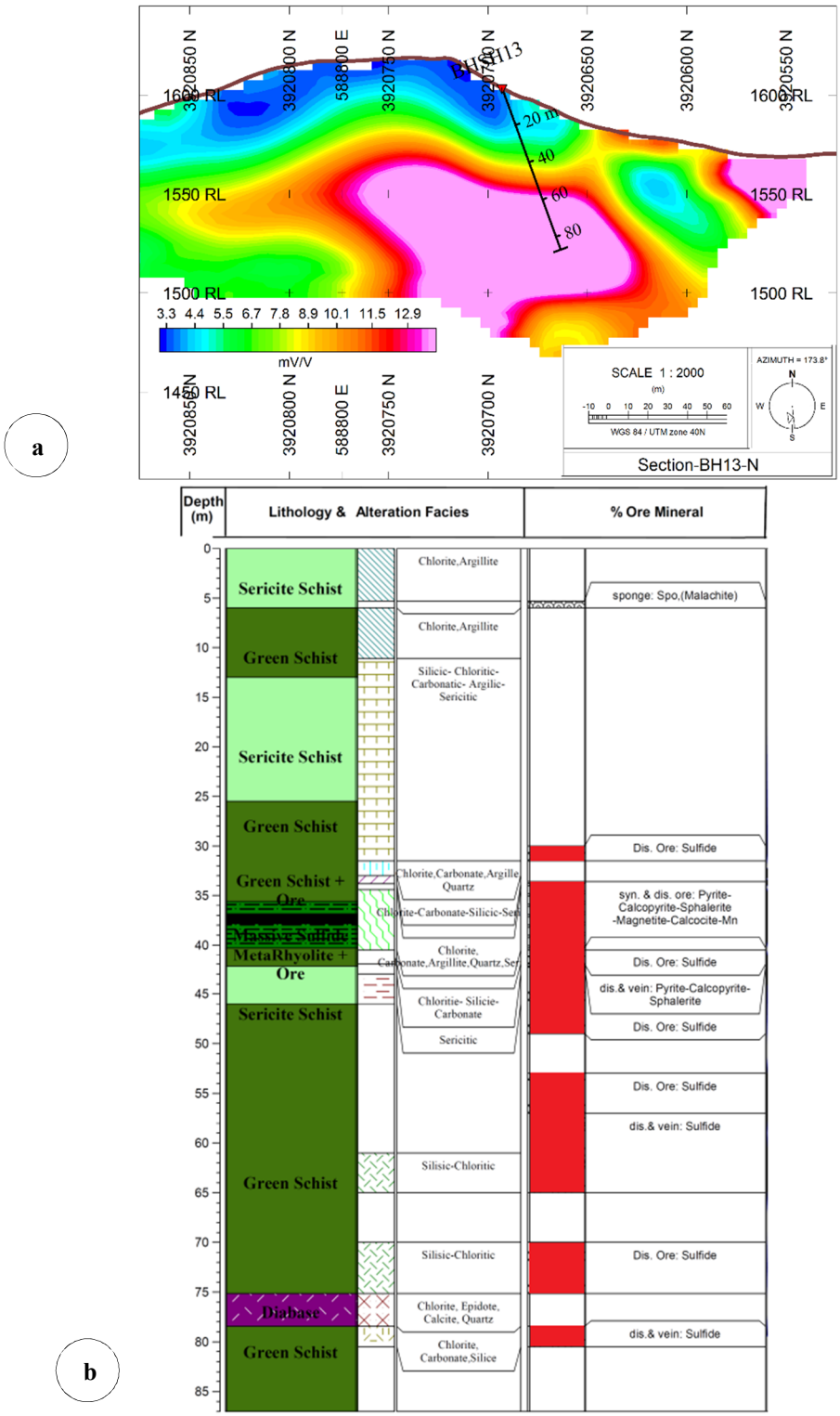

Figure 16. (a) 2D model of IP values and (b) geological log of borehole No. 13 and its corresponding mineralized zones (modified from [32]). As seen, the red-colored box on the logs shows the sulfide zone. The mineralized zones lie at the depths 37-38 m. The geological log approximately confirms the geophysical model. *Dis:* disseminated sulfide; *Syn*: Syngenetic.

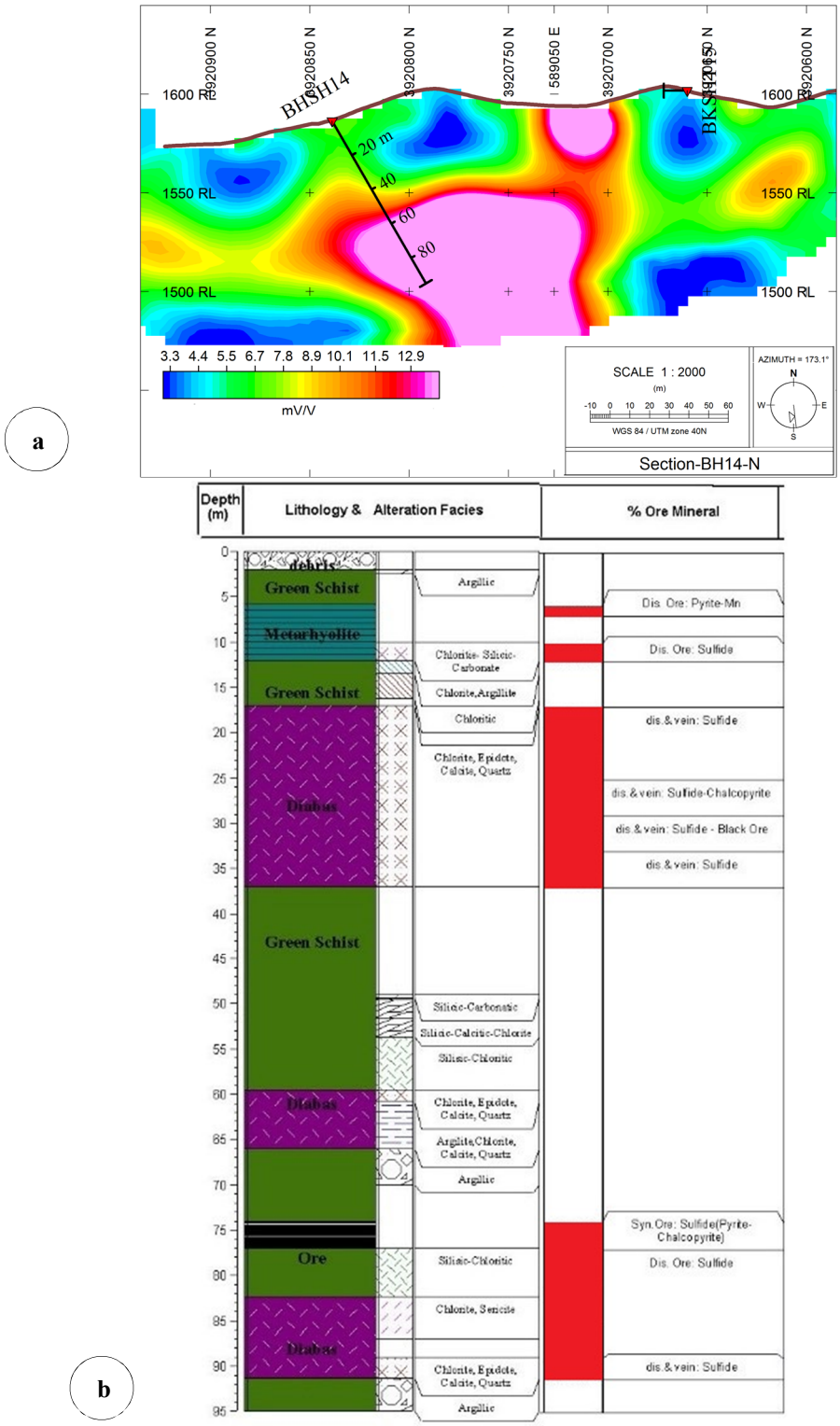

Figure 17. (a) 2D model of IP values and (b) geological log of borehole No. 14 and its corresponding mineralized zones (modified from [32]). As seen, the red-colored box on the logs shows the sulfide zone. The geological log confirms the presence of an ore zone in a depth of around 74untile 77 m, which is also shown in the IP section. *Dis:* disseminated sulfide; *Syn*: Syngenetic.

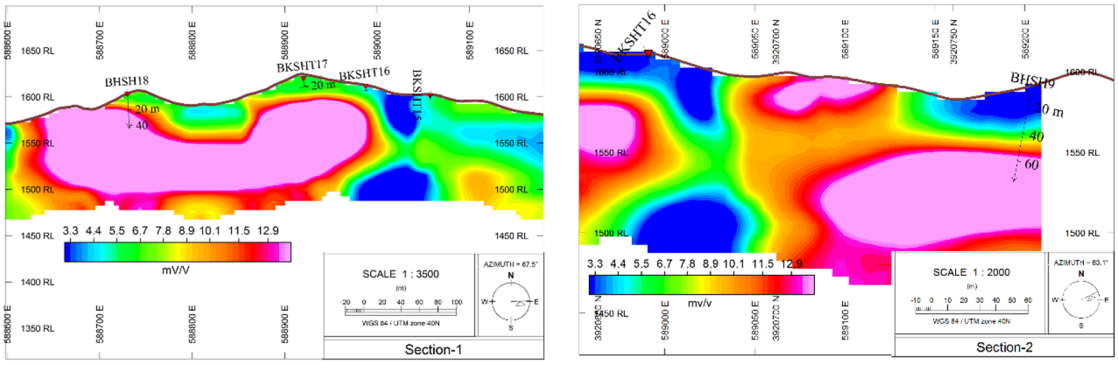

Figure 18. Sections 1 and 2 are drawn along the mineralization zone. The red and purple colors represent the sulfide zones.

It should be noted that in this work, selection of the depth at which the sulfide zone starts is important. The prepared geophysical models were properly cable of selecting this depth.

5. Conclusions

The results of this research work show that the IP data is an appropriate regional variable that can be used in 3D geostatistical modelling of sulfide zones. This 3D modelling can be very effective in delineation of the sulfide and oxide zones. We introduced a new application of IP data through combining the affordable geophysical and geological logging datasets.

The profile spacing in this work was 50-250 m, which is a large distance in the exploration of vein-type gold deposits. Compared to drillings, the geophysical surveys are affordable, and it is suggested to implement a profile spacing of 25 m to obtain a more detailed data. This data provides more accurate variograms and 3D geophysical models that can help engineers delineate the sulfide and oxide zones economically, effectively, and efficiently.

Acknowledgments

We would like to express our sincere gratitudes to the Geological Survey of Iran (NE Branch, Mashhad) for providing the geophysical and drilling datasets. Mehdi Mohammadi Vijeh and Hossein Ferdowsi are appreciated for field and office investigations. We are also grateful to Mehdi Azadi, who revised the first English draft of the manuscript.

References

[1]. Beane, R.E. (1982). Hydrothermal alteration in silicate rocks. In: Titley, S.R. (Ed.), Advances in Geology of the Porphyry Copper Deposits, Southwestern North America. The University of Arizona Press, Tucson. pp. 117-137.

[2]. Berger, B.R., Ayuso, R.A., Wynn, J.C. and Seal, R.R. (2008). Preliminary Model of porphyry Copper Deposits. USGS, Open-File Report. 1321 P.

[3]. Schwartz, G.M. (1947). Hydrothermal alteration in the “porphyry copper” deposits. Economic Geology. 42: 319-352.

[4]. Sillitoe, R.H. (1997). Characteristics and controls of the largest porphyry copper- gold and epithermal gold deposits in the circum-Pacific region. Australian Journal of Earth Science. 44: 373-388.

[5]. Afzal, P., Alghalandis, Y.F., Khakzad, A., Moarefvand, P. and Omran, N.R. (2011). Delineation of mineralization zones in porphyry Cu deposits by fractal concentration–volume modeling. Journal of Geochemical Exploration. 108 (3): 220-232.

[6]. Asghari, O. and Hezarkhani, A. (2008). Appling discriminant analysis to separate the alteration zones within the Sungun porphyry copper deposit. Asian Journal of Applied Sciences. 8 (24): 4472-4486.

[7]. Nash, J.T. (1976). Fluid inclusion petrology–data from porphyry copper deposits and applications to exploration. U. S. Geological Survey professional paper. 907 D:16.

[8]. Roedder, E. (1971). Fluid inclusion studies on the porphyry-type ore deposits at Bingham, Utah, Butte, Montana, and Climax, Colorado. Economic Geology. 66: 98-120.

[9]. Ulrich, T., Gunther, D. and Heinrich, C.A. (2001). The evolution of a porphyry Cu-Au deposit, based on La-ICP-MS analysis of fluid inclusions, Bajo de la Alumbrera, Argentina. Economic Geology. 96: 1743-1774.

[10]. Wilson, A.J., Cooke, D.R., Harper, B.J. and Deyell, C.L. (2007). Sulfur isotopic zonation in the Cadia district, southeastern Australia: exploration significance and implications for the genesis of alkalic porphyry gold-copper deposits. Mineralium Deposita. 42: 465-48.

[11]. Vacquier, V., Holmes, C.R., Kintzinger, P.R. and Lavergne, M. (1957). Prospecting for ground water by

induced electrical polarization. Geophysics. 22 (3): 660-687.

[12]. Marshall, D.J. and Madden, T.R. (1959). Induced polarization, a study of its causes. Geophysics. 24 (4): 790-816.

[13]. Klein, J.D. and Sill, W.R. (1982). Electrical properties of artificial clay-bearing sandstone. Geophysics. 47 (11): 1593-1605.

[14]. Sternberg, B.K. and Oehler, D.Z. (1990). Induced polarization in hydrocarbon surveys: Arkoma basin case histories. INDUCED POLARISATION: Applications and Case histories, 4.

[15]. Kiberu, J. (2002). Induced polarization and Resistivity measurements on a suite of near surface soil samples and their empirical relationship to selected measured engineering parameters. Thesis of Master of Science in Applied Geophysics, International Institute for Geo-Information Science and Earth Observation Enschede, The Netherlands. 119 P.

[16]. Sultan, A.S., Mansour, S.M., Santos, F.M. and Helaly, A.S. (2009). Geophysical exploration for gold and associated minerals, case study: Wadi El Beida area, South Eastern Desert, Egypt. Journal of Geophysics and Engineering. 6 (4): 345.

[17]. Biswas, A., Mandal, A., Sharma, S.P. and Mohanty, W.K. (2014). Delineation of subsurface structures using self-potential, gravity, and resistivity surveys from South Purulia Shear Zone, India: Implication to uranium mineralization. Interpretation. 2 (2): 103-110.

[18]. Biswas, A. and Sharma, S.P. (2016). Integrated geophysical studies to elicit the subsurface structures associated with Uranium mineralization around South Purulia Shear Zone, India: A review. Ore Geology Reviews. 72: 1307-1326.

[19]. Doyle, H.A. (1990). Geophysical exploration for gold- A review. Society of Exploration Geophysicists. 55 (2): 134.

[20]. Urbancic, T.I. and Bailey, R.C. (1989). Statistical techniques applied to borehole geophysical data in gold exploration. Geophysical Prospecting. 36: 752-771.

[21]. Irvine, J.R. and Smith, M.J. (1990). Geophysical exploration for epithermal gold deposits. Journal of Geochemical Exploration. 36 (3): 375-412.

[22]. Dowd, P.A., Johnstone, S.A.W. and Bower, J. (1989). The application of structurally controlled geostatistics to the Hilton orebodies, Mt. Isa, Australia. In: Weiss A (ed.) Proceedings of the 21st APCOM Conference, Chapter 28, Society of Mining Engineers of AIME, Colorado. pp. 275-285.

[23]. Herzfeld, U.C. (1992). Least-squares collocation, geophysical inverse theory and geostatistics: a bird's eye view. Geophysical Journal International. 111 (2): 237-249.

[24]. Kay, M. and Dimitrakopoulos, R. (2000). integrated interpolation methods for geophysical data: application to mineral exploration. Natural Resource Research. 9 (1): 53-64.

[25]. Fisher, T.R., Dagdelen, K. and Turner, A.K. (2005). Modelling 3D grade distributions on the Tarkwa paleoplacer gold deposit, Ghana, Africa. In Geostatistics Banff 2004. Springer, Dordrecht. pp. 439-448

[26]. Schofield, N. (2005). Conditional simulation of grade in a multi-element massive sulphide deposit. Geostat Banff. pp. 449-455.

[27]. Mustapha, H. and Dimitrakopoulos, R. (2009). Modelling complex mineral deposits through high-order spatial cumulants. In: Proceedings Ore body Modelling and Strategic Mine Planning, AusIMM. pp. 319-326.

[28]. De Benedetto, D., Castrignano, A., Sollitto, D., Modugno, F., Buttafuoco, G. and lo Papa, G. (2012). Integrating geophysical and geostatistical techniques to map the spatial variation of clay. Geoderma. 171: 53-63.

[29]. Madan Kav Consulting Co. (2009). Gold exploration in the north of Bardaskan. Unpublished Technical Report, Geological Survey of Iran Press (in Persian).

[30]. Safari, M., Fazlikhani, T. and Jafari, M. (2014). Gold exploration in the Daman Ghor area, Bardaskan. Unpublished Technical Report, Geological Survey of Iran Press (in Persian).

[31]. Monazzami Bagherzadeh, R., Karimpour, M.H., Lang Farmer, G., Stern, C.R., Santos, J.F., Rahimi, B. and Heidarian Shahri, M.R. (2015.) U-Pb zircon geochronology, petrochemical and Sr–Nd isotopic characteristic of Late Neoproterozoic granitoid of the Bornaward Complex (Bardaskan-NE Iran). Journal of Asian Earth Science. 111: 54-71.

[32]. Safari, M. and Azmi, H. (2018). General exploration of massive sulfide deposits in the Kelateh Shojae area, Bardaskan. Unpublished Technical Report, Geological Survey of Iran Press (in Persian).

[33]. Rahimi, H., Asghari, O., Hajizadeh, F. and Meysami, F. (2018). Investigation of linear and non-linear estimation methods in highly-skewed gold distribution. Journal of Mining and Environment. 9 (4): 967-979.

[34]. Mohammadi Vijeh, M. (2010). Exploration of polymetallic deposits using the IP-RS surveys. Unpublished Technical Report, Geological Survey of Iran Press (in Persian).

[35]. Calder, C. and Cressie, N.A. (2009). Kriging and variogram models. Elsevier.

[36]. Armstrong, M. and Delfiner, P. (1980). Towards a more robust variogram: A case study on coal. Fontainebleau: Springer.

[37]. Cressie, N. and Hawkins, D.M. (1980). Robust estimation of the variogram: I. Journal of the International Association for Mathematical Geology. 12 (2): 115-125.

[38]. Wackernagel, H. (2013). Multivariate geostatistics: an introduction with applications. Springer Science & Business Media.

[39]. Armstrong, M. (1998). Basic linear geostatistics. Springer Science & Business Media.

[40]. Journel, A.G. and Huijbregts, C.J. (1978). Mining geostatistics (Vol. 600). London: Academic press.

تخمین زمین‌آماری برای جداسازی زون‌های اکسیدی و سولفیدی با استفاده از داده‌های ژئوفیزیکی؛ مطالعه موردی کانسار طلای رگه‌ای چهاربخشی، شمال شرق ایران

حسن عزمی*، پرویز معارف‌وند و عباس مقصودی

دانشکده مهندسی معدن و متالورژی، دانشگاه صنعتی امیرکبیر، ایران

ارسال ۲۰۱۹/۱/۲، پذیرش ۲۰۱۹/۳/۱۳

* نویسنده مسئول مکاتبات: azmi@aut.ac.ir

چکیده:

جداسازی مناطق اکسیدی و سولفیدی در ذخایر معدنی، به ویژه در ذخایر طلا، یکی از ضروری‌ترین مراحل در یک پروژه اکتشافی است که به طور معمول با استفاده از نتایج حفاری انجام می‌شود. از آنجایی که در بیشتر پروژه‌های اکتشافی داده‌های حفاری محدودی در دسترس است، استفاده از داده‌های ژئوفیزیکی می‌تواند خطای جدایش مناطق سولفیدی و اکسیدی را کاهش دهد. بدین منظور، در این پژوهش، یک مدل سه‌بعدی از داده‌های پلاریزاسیون القایی با استفاده از تکنیک کریجینگ معمولی تولید شد. سپس نتایج مدل‌سازی با داده‌های حفاری مقایسه شد. نتایج به دست آمده نشان داد که مدل‌های ژئوفیزیکی سه‌بعدی به درستی مناطق سولفیدی و اکسیدی را مشخص می‌کند. این پژوهش، کاربرد جدیدی از داده‌های پلاریزاسیون القایی برای جداسازی مناطق اکسیدی و سولفیدی طلا معرفی می‌کند. علاوه بر این، واریوگرافی انجام شده در این کار نشان می‌دهد که حداقل فاصله پروفایل بین آرایه‌های دوقطبی-دوقطبی پلاریزاسیون القایی بایستی به ۲۵ متر کاهش یابد. نتایج این پژوهش می‌تواند به خوبی تلفیق نتایج ژئوفیزیکی و زمین‌شناسی در مدل‌سازی کانسارهای طلا را بهبود بخشد.

کلمات کلیدی: زون‌های اکسیدی و سولفیدی، مدل ژئوفیزیکی، ذخایر رگه‌ای طلا، کریجینگ معمولی.